Long-term creep life prediction for Grade 22 (2.25Cr-1Mo) steels

MT Whittaker and B Wilshire

Materials Research Centre, School of Engineering, Swansea University, Swansea. SA2 8PP, UK.

Abstract

Using new data analysis procedures, 100,000h creep strengths are estimated by extrapolation of stress rupture values with creep lives less than 5000h for Grade 22 tube as well as for annealed/tempered and quenched/tempered plates. In addition to allowing accurate prediction of long-term strengths, the resulting property sets can be discussed sensibly in terms of the deformation and damage processes controlling creep and creep fracture.

Keywords: Creep, creep fracture, mechanisms, Wilshire equations.

1. Introduction

Large-scale components and structures in power and petrochemical plant are normally designed on the basis that creep fracture should not occur within the planned design life, usually 250,000h. Because of the long timescales involved, decisions are generally made from the 'allowable tensile stresses', which are the stresses which cause failure in 100,000h at the service temperatures. Even so, for reasons of economy and CO_2 emissions, there are now international efforts being made to raise plant operating temperatures to reduce fuel consumption. Unfortunately, this requires new high-performance alloy steels, but the problems then remain of the high costs and extended durations of the creep testing programmes needed to obtain the necessary design data.

Over the last 50 years and more, major attempts have been made to devise procedures which permit accurate estimation of long-term properties from short-term results. Beginning with the parametric relationships introduced in the 1950s [1-3], many alternative data extrapolation methods have been evolved more recently, but none of these have proved entirely successful [4]. However, a new approach has now been

produced, termed the Wilshire equations [5-8]. This concept defines the dependence of the creep rupture life (t_f) on stress (σ) and temperature (T) as

$$(\sigma/\sigma_{TS}) = \exp \{-k_1 [t_f . \exp (-Q_c^*/RT)]^u\} \quad (1)$$

where R=8.314 $Jmol^{-1}K^{-1}$, t_f is in secs and σ is in MPa. Similar equations then quantify the minimum creep rates ($\dot{\varepsilon}_m$) and the times to specific strains (t_ε). In these cases, σ_{TS} is the ultimate tensile strength determined in high-strain-rate ($10^3 s^{-1}$) tests carried out at the various creep temperatures studied for each batch of material. Because σ_{TS} is the highest stress which can be applied at the creep temperature, eqn (1) has the obvious advantage that $t_f \rightarrow 0$ as $(\sigma/\sigma_{TS}) \rightarrow 1$, while $t_f \rightarrow \infty$ as $(\sigma/\sigma_{TS}) \rightarrow 0$. It is then a straightforward matter to compute the values of k_1, u and Q_c^* from the $t_f/\sigma/T$ plots measured for any batch of material [5-8].

Eqn (1) has proved successful in allowing measured 100,000h creep strengths to be predicted from test results with maximum lives of 5000h for a range of power plant steels, including ferritic [8], bainitic [7] and martensitic products [6]. Even so, to verify this approach, the present work focuses on bainitic Grade 22 (2.25Cr-1Mo) steels, where a dispersion of fine molybdenum carbide precipitates provide the high temperature strength, while the chromium confers resistance to oxidation during plant exposure.

Grade 22 steels have been extensively used for superheater and reheater tubing, as well as for high-temperature headers and piping for over half a century. Consequently, major sets of creep rupture data are already available to check the accuracy of the long-term predictions now made by extended extrapolation of short-term measurements. Moreover, information has been systematically gathered by the National Institute for Materials Science (NIMS), Japan, on Grade 22 steels supplied in different conditions, including

a) quenched and tempered plate for pressure vessels [9],
b) normalized and tempered plate for boiler and pressure vessels [10] and
c) tube for boilers and heat exchangers [11],

with the creep rupture properties supplemented by detailed microstructural studies of as-received and crept materials [12].

Using this broad range of information, the present aims are therefore to assess the predictive capabilities of eqn (1) in relation to the processes of deformation and failure which control the creep and creep fracture properties of Grade 22 steels.

2. Power Law Creep Fracture Behaviour

All of the materials considered by NIMS [12] were well within the composition limits (wt %) set for Grade 22 steels, namely, 0.05-0.15 C (max); 0.3-0.6Mn; 0.025 P (max); 0.025 S (max); 0.5 Si; 1.9-2.6 Cr; 0.87-1.3 Mo. The heat treatments received were [12]

a) 1203K for 6h before water quenching and tempering firstly for 6h at 908K then air cooling and secondly for 2h at 873K before furnace cooling of the quenched/tempered plate.
b) 1203K for 1h and air cooled, 1013K for 2h then air cooled and 973K for 4h before furnace cooling of the annealed/tempered plate and
c) 1203K for 20 mins, then cooled to 993K for 130 mins before air cooling of the tube,

These schedules produced ferrite-bainite microstructures with around 80% ferrite regions in the tube and almost exclusively bainite microstructures with both the quenched/tempered and annealed/tempered plate [12,13].

The NIMS creep rupture tests were carried out [8-12] at 723 to 923K (450-650°C) at stresses such that the longest tests for all three product types lasted more than 100,000h, so extrapolation was not necessary to calculate the allowable creep strengths. In line with common practice, the stress and temperature dependencies of the creep lives were then presented [12] using standard power law equations, as

$$M/t_f = \dot{\varepsilon}_m = A\,\sigma^n \exp(-Q_c/RT) \qquad (2)$$

where the parameters (A and M), the stress exponent (n) and the activation energy for creep (Q_c) vary in different stress/temperature regimes. Thus, as evident from the results for the quenched and tempered material in Fig. 1, a decrease from $n \cong 14$ to $n \cong 3.5$ occurs with decreasing stress and increasing temperature over the ranges covered, with Q_c varying from approximately 100 to 350 $kJmol^{-1}$.

As shown in Fig. 2, the results for all three product types were plotted [12] as functions of the Larson-Miller parameter [1], namely

$$P_{LM} = T_K (20 + \log t_f) \qquad (3)$$

where T_K is in Kelvin and t_f is in hours. Clearly, all three heat-treatments give similar performances at low stresses, with the quenched/tempered material producing longer creep lives at stresses above about 80MPa.

Because of the long-term measurements completed by NIMS for all three products, the Larson-Miller method should allow accurate estimation of 100,000h creep rupture strengths. Even so, with σ_{TS} values determined at the creep temperatures [9-11], it is interesting to consider the effects of amending eqn (2) to demonstrate the variations in t_f with (σ/σ_{TS}) as

$$M/t_f = \dot{\varepsilon}_m = A^*(\sigma/\sigma_{TS})^n \,.\, \exp(-Q_c^*/RT) \qquad (4)$$

where $A^* \neq A$ and $Q_c^* \neq Q_c$. As illustrated in Fig.3, eqn (4) superimposes the data sets for each material onto single curves. Moreover, this procedure eliminates the variability in Q_c found with eqn (1), producing a fixed Q_c^* value of $280kJmol^{-1}$, coinciding with the activation energy for matrix self diffusion in the Grade 22 steels. Yet, while a fixed Q_c^* value is obtained, eqn (4) does not eliminate the changes in n found with eqn (2), as evident from Figs. 1 and 3. These n value changes mean that the plots in Figs. 1, 2 and 3 all curve in an unpredictable manner, so that 250,000h creep strengths cannot be estimated unambiguously by extrapolation of t_f values up to 100,000h.

3. Application of New Data Fitting Procedures

To evaluate the effectiveness of eqn (1), the (σ/σ_{TS})/creep life data at different temperatures for each heat treatment were superimposed onto single lines with Q_c^*=280kJmol^{-1} (as in Fig.3). The values of k_1 and u in eqn (1) were then determined by plotting $\ln[t_f.\exp(-Q_c^*/RT)]$ as functions of $\ln[-\ln(\sigma/\sigma_{TS})]$. Different behaviour patterns were found for each heat treatment. These can be summarised as follows.

(a) For the quenched and tempered plate, a plot of $\ln[t_f.\exp(-Q_c^*/RT)]$ against $\ln[-\ln(\sigma/\sigma_{TS})]$ was essentially a single straight line, with k_1= 49.1 and u = 0.157 (Fig. 4).

(b) For the normalized and tempered plate, only a single break was found in the $\ln[t_f.\exp(-Q_c^*/RT)]$ against $\ln[-\ln(\sigma/\sigma_{TS})]$ plot, with a change from k_1= 65.5 and u = 0.165 at high stresses (when $\sigma > 0.4\sigma_{TS}$) to k_1= 22.2 and u = 0.123 when $\sigma < 0.4\sigma_{TS}$ (Fig.5). Hence, the t_f values when $\sigma<0.4\sigma_{TS}$ are longer than expected by extrapolation of data when $\sigma>0.4\sigma_{TS}$.

(c) For the tube material, the $\ln[t_f.\exp(-Q_c^*/RT)]$ against $\ln[-\ln(\sigma/\sigma_{TS})]$ plots showed three distinct regions (Fig.6). The high stress results (where $\sigma > 0.4\sigma_{TS}$) gave k_1= 3584 and u = 0.307. In the intermediate stress range, as with the normalized and tempered plate, the t_f values were longer than expected by direct extrapolation of the high stress t_f measurements, with k_1 = 6.45 and u = 0.071 . In the low stress range, (when $\sigma<0.2\sigma_{TS}$), the t_f data become significantly shorter than those estimated by direct extrapolation of the intermediate stress results, with k_1= 624 and u= 0.294.

Although Figs. 4, 5 and 6 show the stress rupture values recorded at all temperatures for the three different heat treatments, in all cases, the lines drawn to determine k_1 and u were calculated for results with t_f < 5000h. Even so, by inserting the values of k_1, u and Q_c^* into eqn (1), the predicted stress/creep life curves fit well with the measured data for all three product forms (Fig.7). Thus, as with other power plant steels [6-8], eqn (1) allows extended extrapolation of short term t_f measurements to predict long-term stress rupture properties accurately, provided that creep fracture is the dominant failure mode. Moreover, for Grade 22 steels, the 100,000h creep rupture strengths are very similar for all three starting microstructures (Fig.7).

4. Creep Deformation Processes

With n>4, it is universally agreed that creep occurs by diffusion-controlled generation and movement of dislocations. Indeed, recent studies have suggested that dislocation mechanisms are dominant even when $n \cong 1$ [14]. However, the detailed dislocation processes taking place depend on microstructural changes during creep and on whether $\sigma > \sigma_{PS}$, where σ_{PS} is the proof stress of each batch of material at the creep temperature [9-11]. Thus, as evident from the NIMS data [9-11] in Fig.8, the initial extensions on loading (ε_0) are fully elastic up to about $0.85\sigma_{PS}$, but increase rapidly as the plastic component becomes progressively greater when $\sigma > 0.85\sigma_{PS}$ ($\sigma > 0.4\sigma_{TS}$).

It must be expected that σ_{PS} is slightly greater than σ_Y, where σ_Y is the yield stress of each steel batch at the appropriate test temperature, seemingly with $\sigma_Y \cong 0.85\sigma_{PS}$ (Fig.8). As previously found for pure copper [5] and for a 1Cr-0.5Mo steel [8], with stresses such that $\sigma > \sigma_Y$, dislocations multiply rapidly during the initial plastic strain on loading. In contrast, when $\sigma < \sigma_Y$, creep must occur not by the generation of new dislocations but by the movement of dislocations pre-existing in the as-received microstructures, with deformation confined to the grain boundary zones, i.e. zone deformation comprises grain boundary sliding and associated dislocation movement in grain regions adjacent to the boundaries [5,8]. Thus, the creep rates are slower and the creep lives are longer when $\sigma < \sigma_Y$, compared with the values anticipated by linear extrapolation of data collected when $\sigma > \sigma_Y$.

In the context that a break should occur in the log t_f/log σ plots when the stress falls from above to below σ_Y ($\cong 0.85\sigma_{PS}$), it is a straightforward matter to rationalize the behaviour patterns found when eqn (1) is applied to the stress rupture data for Grade 22 steels produced using different heat treatments:

(a) With the quenched and tempered plate, all tests were carried out at stresses less than $0.85\sigma_{PS}$, so deformation is always confined to the boundary zones. Hence, there is no break in the plot of $\ln[t_f.\exp(-Q_c^*/RT)]$ against $\ln[-\ln(\sigma/\sigma_{TS})]$, as shown in Fig.4. Specifically, this material remains as

bainite, but with the carbide particles coarsening significantly with increasing time and temperature, particularly on the grain boundaries [12].

(b) With the annealed and tempered plate, a single break occurs at $\sigma \cong 0.4\sigma_{TS} \cong 0.85\sigma_{PS}$ (Fig.5), so the creep lives become longer when grain deformation is restricted so that creep occurs by grain boundary zone deformation. Again, the microstructures remain bainitic, but with the carbides coarsening as found for quenched and tempered plate [12].

(c) With the tube material, two breaks are found in the $\ln[t_f.\exp(-Q_c^*/RT)]$ against $\ln[-\ln(\sigma/\sigma_{TS})]$ plot (Fig.6). The first break occurs when σ falls from above to below about $0.85\sigma_{PS}$, when longer creep lives are again observed when deformation is confined to the grain boundary zones at the lower stresses. Even so, a second break occurs when $\sigma \cong 0.35\sigma_{PS}$ ($\cong 0.2\sigma_{TS}$). This is a consequence of the bainitic regions degrading to ferrite and molybdenum carbide particles, with very coarse carbides along grain boundaries. As a result, when $\sigma < 0.2\ \sigma_{TS}$, the creep rates are faster and the creep lives are substantially shorter in tests of long duration at 873K and above than would be expected by direct extrapolation of results when $0.85\sigma_{PS} > \sigma > 0.35\ \sigma_{PS}$ (Fig.6).

The present analysis therefore shows that no break occurs in Fig.4 for the quenched/tempered steel (because σ is always less than $0.85\sigma_{PS}$), whereas gradient changes occur when σ falls from above to below $0.85\sigma_{PS}$ ($\cong \sigma_Y$) such that the low stress t_f values are longer than those expected from the high stress results for the tube and annealed/tempered samples (Figs. 5 and 6). This observation is fully compatible with the behaviour pattern found using the Larson-Miller method (Fig.2). Even so, for all three heat treatments, the gradual loss of creep strength with increasing test duration at the higher creep temperatures is attributable to gradual coarsening of the molybdenum carbide particles. This is evident from the fact that plots of $\ln[t_f.\exp(-Q_c^*/RT)]$ against both stress (Fig.7) and hardness within the gauge length after creep (Fig.9) are very similar.

5. Creep Fracture Processes

While creep occurs by diffusion-controlled dislocation movement, with the detailed processes dependent on microstructural changes and test conditions, distinct differences in creep fracture behaviour are found with the tube and annealed/tempered plate products and with the quenched/tempered material [9-11]. These differences in failure mechanism can be inferred from plots of the reduction in area at fracture (RoA) and the total creep elongation (ε_f) as functions of log [$t_f.\exp(-Q_c^*/RT)$] in Figs. 10 to 12 inclusive.

With the tube and annealed/tempered plate samples, under all test conditions covered, the RoA values were usually in excess of 0.8, whereas the majority of the ε_f results were in the range 0.2 to 0.6 (Fig.9 and 10). Thus, with RoA> ε_f, extensive necking always precedes failure, which takes place in a transgranular manner [12]. Similar results were obtained at 723 and 923K for the quenched and tempered plate, but very different results were observed at 773 to 873K (Fig.11). Specifically, at 773 to 873K, selected stress levels gave very low values of both RoA and E_L, suggesting that fracture occurs in an intergranular manner, a view supported by the NIMS metallographic studies [12]. Even so, these differences in failure mode are insufficient to significantly alter the long-term stress/creep life relationships, which appear to be similar for all three heat-treatments given to the Grade 22 testpieces (Fig.7).

6. Conclusions

A study has been made of the creep fracture behaviour at 723 to 923K of Grade 22 (2.25Cr-1Mo) steels produced in the form of tube, annealed/tempered plate and quenched/tempered plate. For all three product forms, NIMS creep rupture properties [9-12] at stresses giving creep curves up to 5000h were analysed using the recently devised relationship [5-8].

$$\left(\sigma / \sigma_{TS}\right) = \exp\left\{-k_1\left[t_f \exp(-Q_C^* / RT)\right]^u\right\}$$

where σ_{TS} is the ultimate tensile stress at each creep temperature for individual batches of steel. In this way, data sets at the different creep temperatures were superimposed onto single curves for each product, giving $Q_c^*=280kJmol^{-1}$, the activation energy for matrix self diffusion. By determining the values of k_1 and u for each batch of material, this relationship allowed extended extrapolation of results for creep lives up to 5000h to accurately predict NIMS stress rupture data for times exceeding 100,000h, provided that creep failure is the dominant failure mode. On this basis, it appears that this new procedure should allow cost-effective estimation of 100,000h allowable stresses for newly developed steels. Moreover, consideration of the stress rupture properties, together with the reductions in area and total elongations to failure, permit the observed behaviour patterns to be discussed sensibly in terms of the dislocation processes controlling creep strain accumulation and the various damage processes causing fracture as the microstructures evolve with increasing test duration and temperature.

References

[1] F.R. Larsson and J.Miller: Trans ASME, 1952, **74**, 765-775.

[2] S.S. Manson and A.M. Haferd: NASA TN2890, 1953.

[3] R.L. Orr, O.D. Sherby and J.E. Dorn: Trans ASM, 195, **46**, 113-128.

[4] S.R. Holdsworth et al: in 'Creep and fracture in high temperature components – design and life assessment issues' (Ed. A. Shibli et al), 280-393; 2005, London, DEStech Publ. Inc.

[5] B. Wilshire and A.J. Battenbough, *Mater. Sci. Eng A.*, 2007, **443A**, 156-166.

[6] B. Wilshire and P.J. Scharning, *Int. Mater. Rev.*, 2008, **53,** 91-104.

[7] B. Wilshire and P.J. Scharning, *Mater. Sci. Tech.*, 2008, **24**, 1-9.

[8] B. Wilshire and P.J. Scharning, *Int. J. Press. Vessels and Piping*, 2008, **85** 739-743.

[9] NIMS Creep Data Sheet No 36B. 2003. Data sheets on the elevated temperature properties of quenched and tempered 2.25Cr-1Mo steel plates for pressure vessels (ASTM A542/A542M)

[10] NIMS Creep Data Sheet No 11B. 1997. Data sheets on the elevated temperature properties of normalized and tempered 2.25Cr-1Mo steel plates for boilers and pressure vessels (SCMV 4 NT)
[11] NIMS Creep Data Sheet No 3B. 1986. Data sheets on the elevated temperature properties of 2.25Cr-1Mo steel for boiler and heat exchanger seamless tubes (STBA 24)
[12] NIMS Creep Data Sheet: Metallographic atlas of long-term crept materials, No M-4, 2005.
[13] J.D. Parker; The Grade 22 low alloy steel handbook, EPRI, Palo Alto, CA; 2005. 1012840.
[14] B. Wilshire and M.T. Whittaker: Mater. Sci. Technol., 2009, In Press.

Figure captions

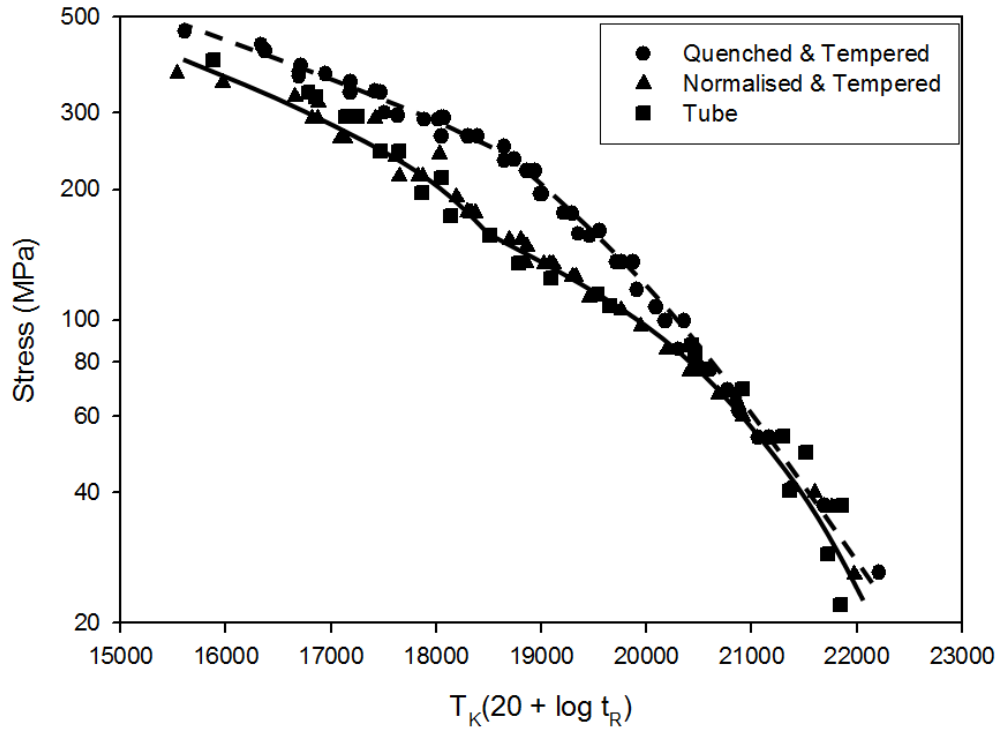

Fig.1. The stress dependence of the creep rupture lives at 723 to 923K for quenched and tempered Grade 22 plate [9]. The solid lines are calculated using eqn (1).

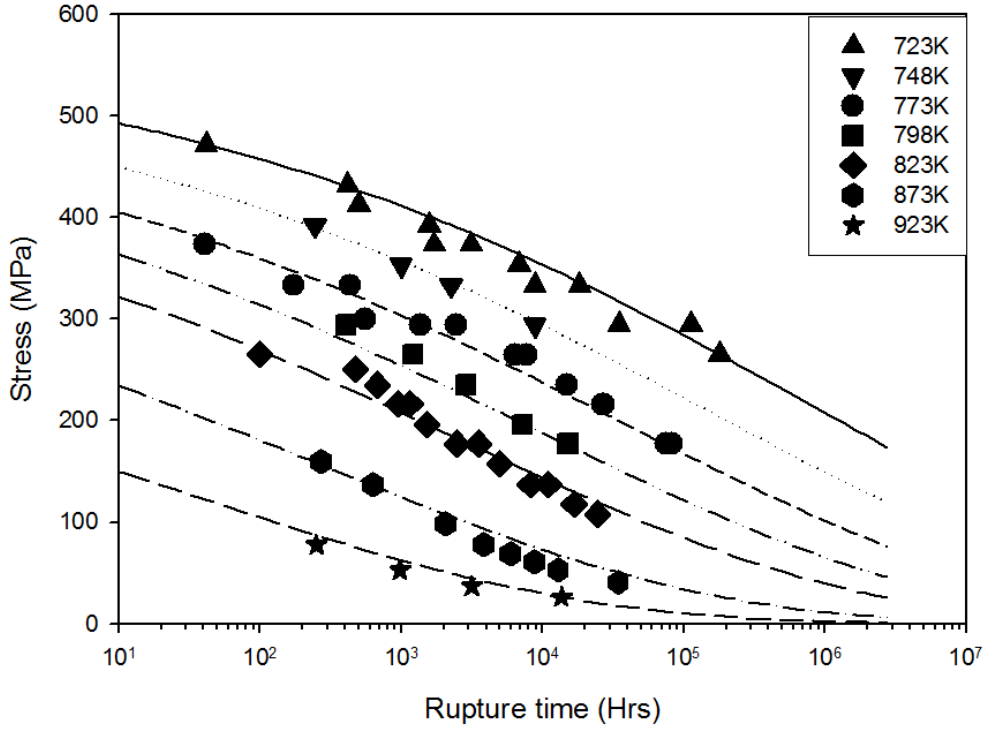

Fig. 2. The creep rupture strength plotted against the Larson-Miller parameter (eqn (3), with C=20) for Grade 22 tube and annealed/tempered plate, as well as for quenched/tempered plate [12]. Temperature T_K is in Kelvin and t_f is in hours. Similar curves are observed for the tube and annealed/tempered products, whereas the quenched/tempered material shows higher strengths in short term tests, while the results for all three heat treatments are comparable as the test durations approach 100,000h. It should also be noted that the creep lives are longer at stresses less than about 150MPa than would be expected by direct comparison of the data collected when σ>150MPa for the tube and normalized/tempered samples.

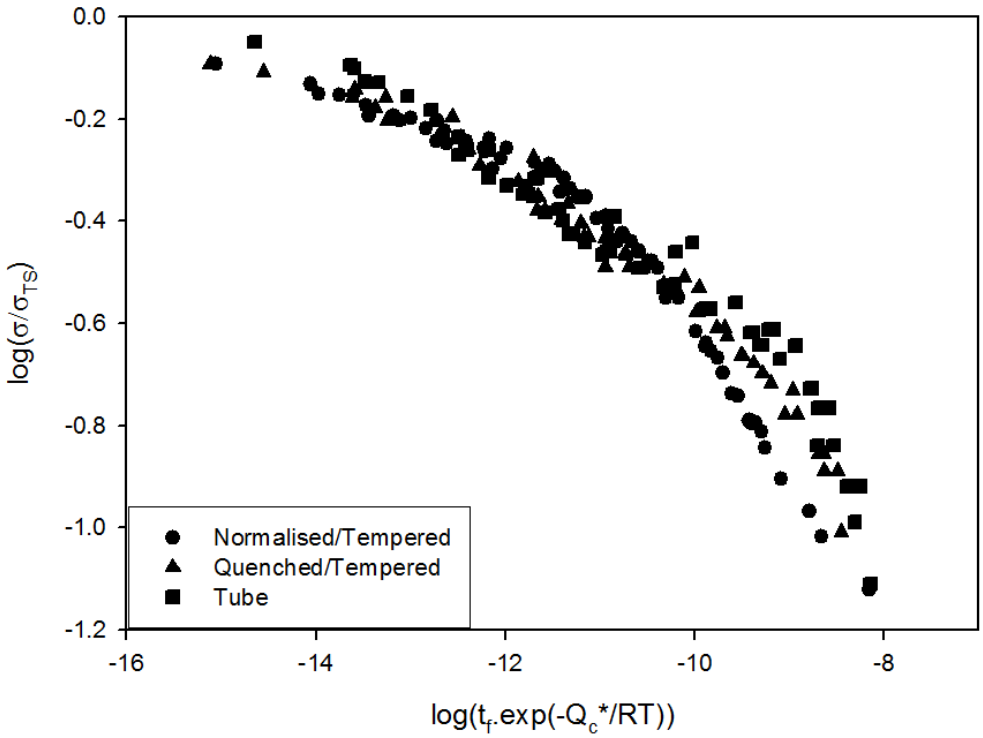

Fig.3. The dependencies of log [t_f.exp(-Q_c^*/RT)], with Q_c^*=280kJmol^{-1}, on log(σ/σ_{TS}) for Grade 22 tube and annealed/tempered plate, as well as for quenched/tempered plate.

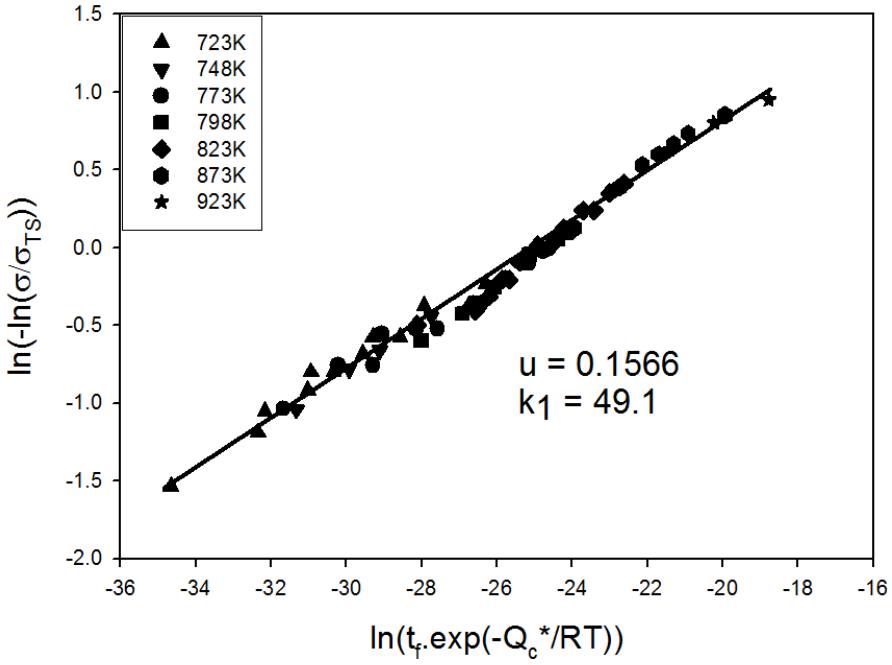

Fig.4. The dependence of $\ln[t_f.\exp(-Q_c^*/RT)]$on $\ln[-\ln(\sigma/\sigma_{TS})]$, with $Q_c^*=280kJmol^{-1}$, for quenched and tempered Grade 22 plate.

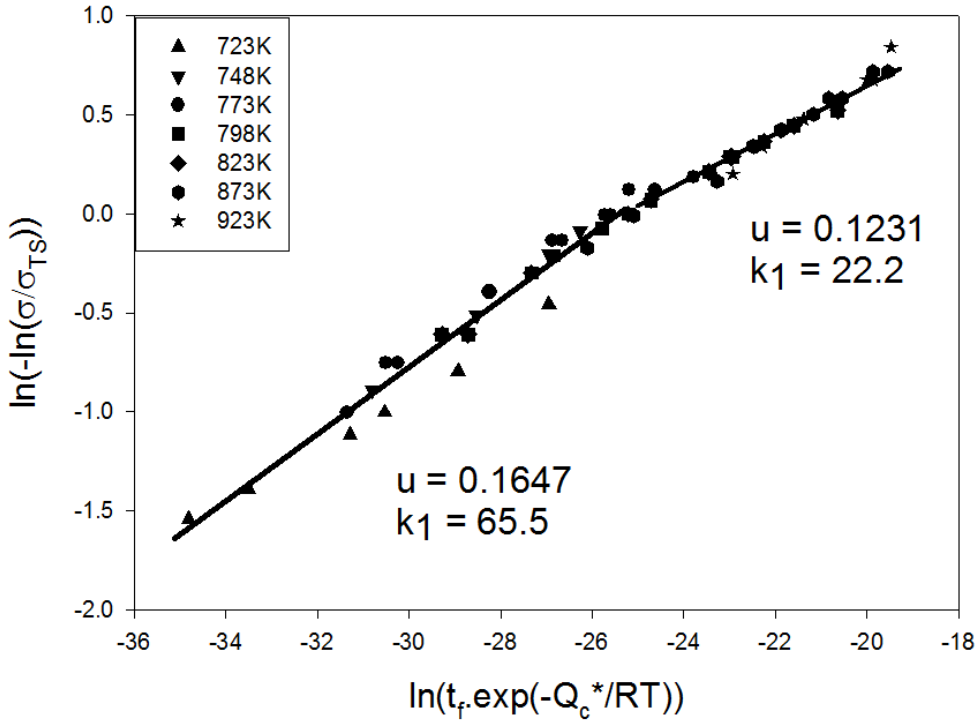

Fig.5. The dependence of $\ln[t_f.\exp(-Q_c^*/RT)]$on $\ln[-\ln(\sigma/\sigma_{TS})]$, with $Q_c^*=280kJmol^{-1}$, for annealed and tempered Grade 22 plate.

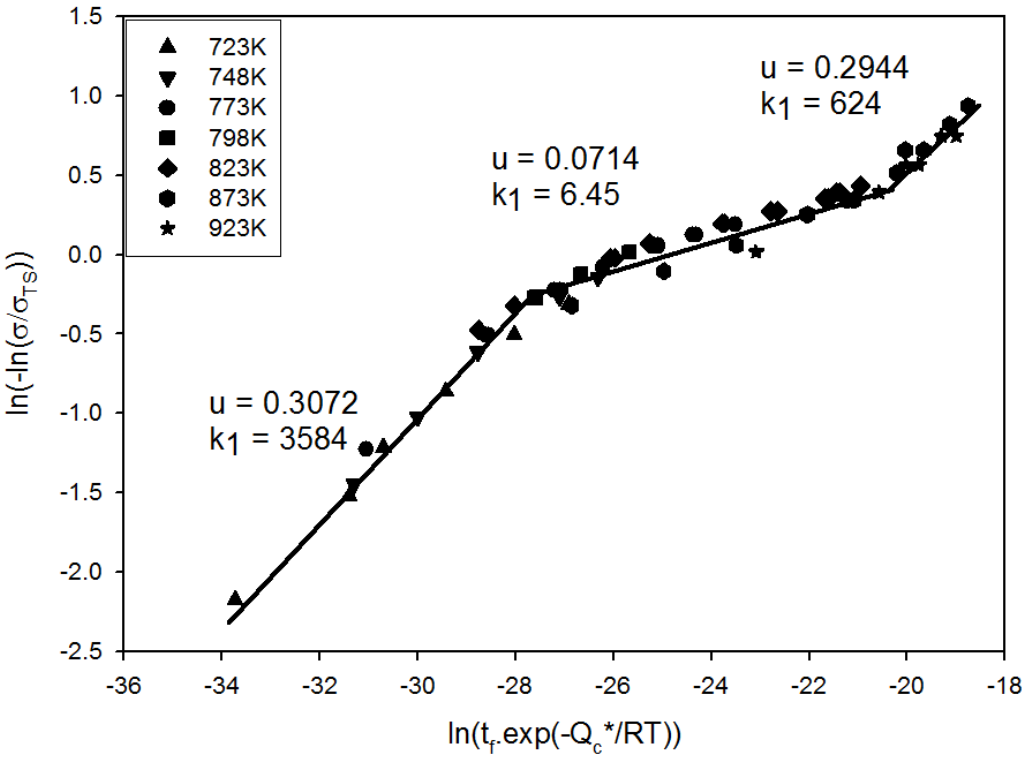

Fig.6. The dependence of $\ln[t_f.\exp(-Q_c^*/RT)]$on $\ln[-\ln(\sigma/\sigma_{TS})]$, with $Q_c^*=280 kJmol^{-1}$, for Grade 22 tube.

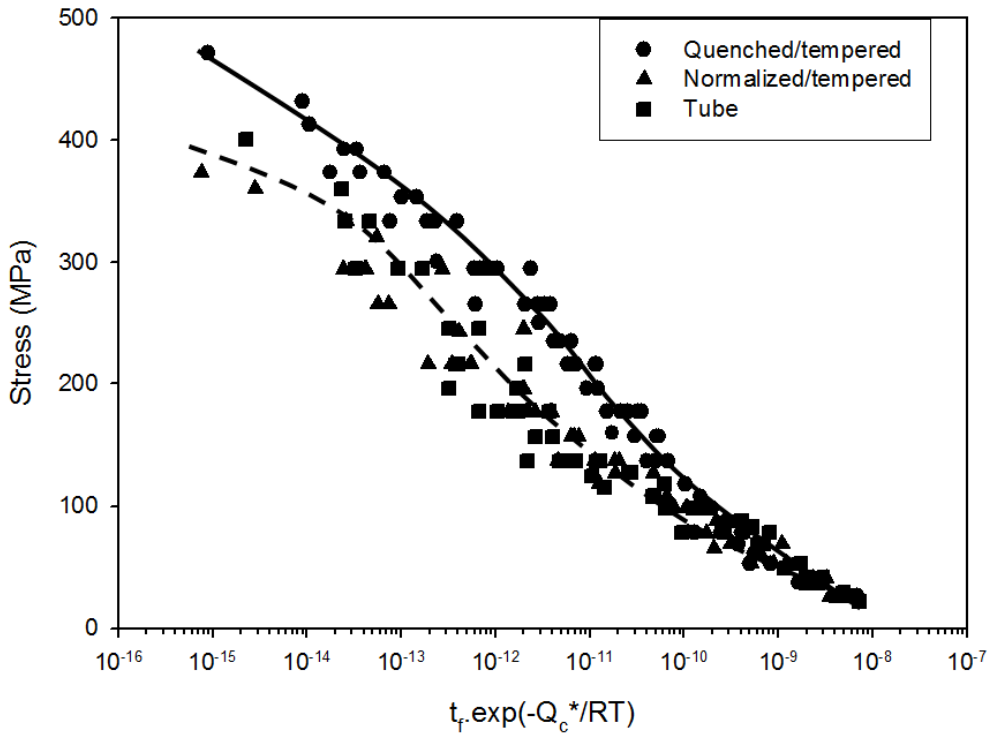

Fig.7. The stress dependence of $\log[t_f.\exp(-Q_c^*/RT)]$, with $Q_c^*=280 kJmol^{-1}$, for Grade 22 tube and annealed/tempered plate, as well as for quenched/tempered plate. The curve (solid line) shows that eqn (1), using the derived values of k_1, u and Q_c^*, accurately describes the creep fracture behaviour of the quenched/tempered material. In contrast, the broken curve presents the averaged results obtained by applying eqn (1) to the data recorded for the tube [11] and annealed/tempered plate [10], illustrating the similarities in creep rupture strengths found for these two products.

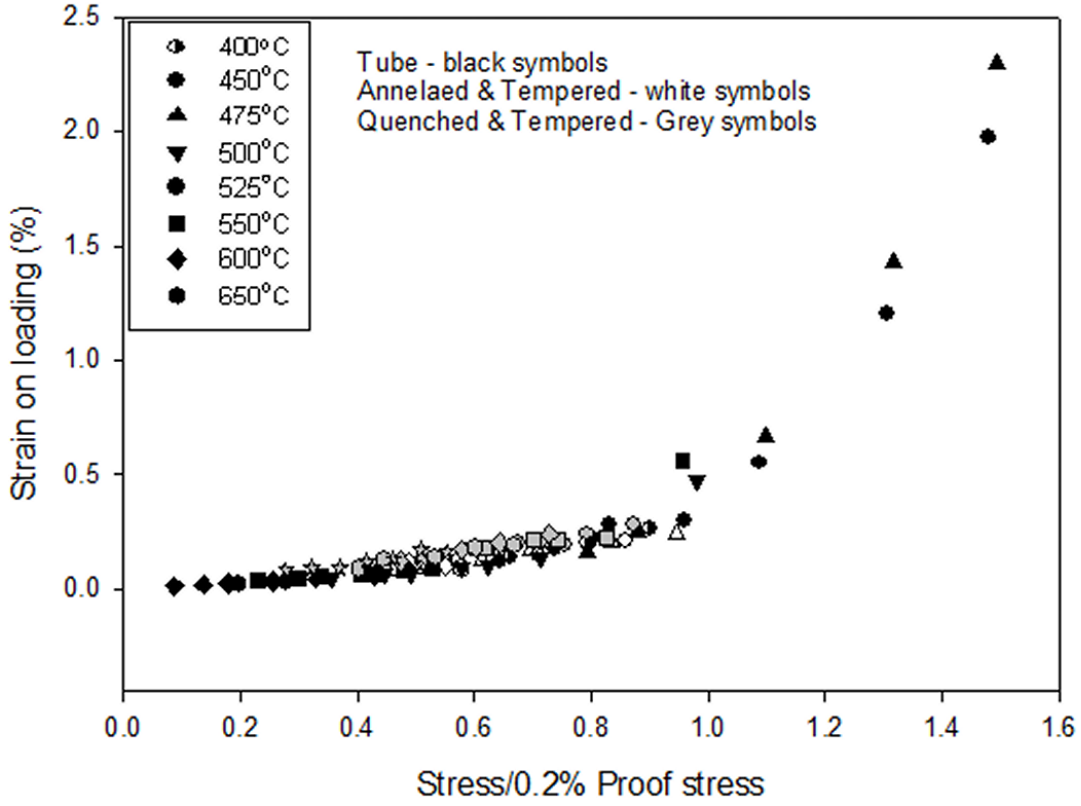

Fig.8. The dependence of the initial strain on loading (ε_0) on σ/σ_{PS}, where σ_{PS} is the proof stress determined from high-strain-rate tests at the creep temperatures for each batch of material. Clearly, ε_0 increases elastically with stress up to about $0.85\sigma_{PS}$, then increases very rapidly as the plastic component of ε_0 rises when $\sigma>0.85\sigma_{PS}$.

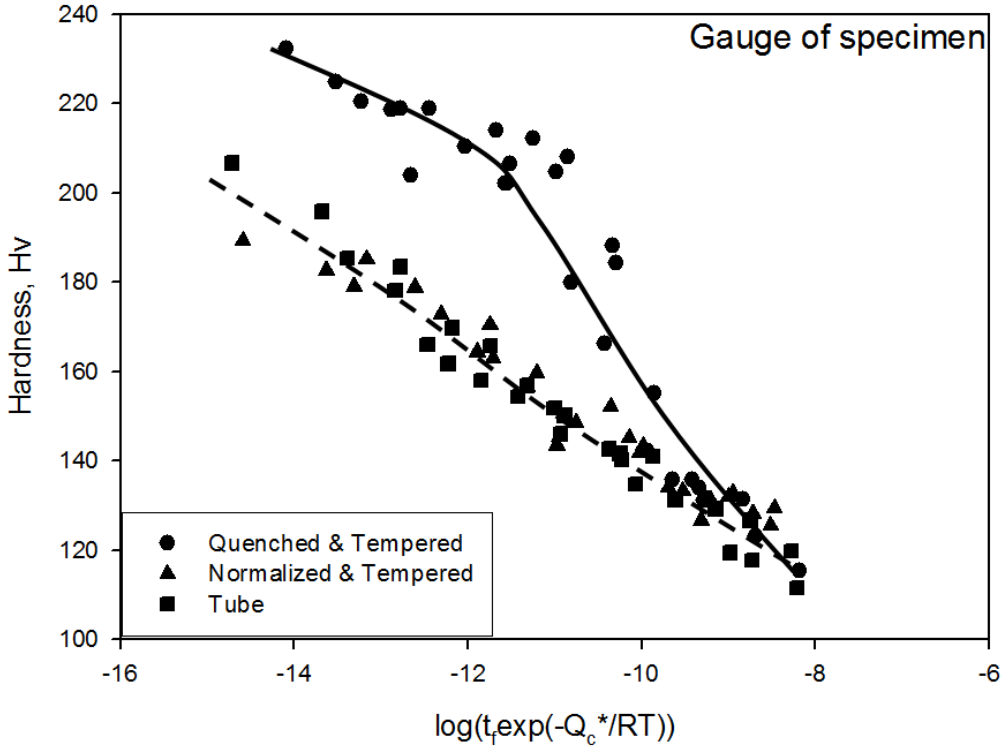

Fig.9 The dependencies of the hardness within the gauge length of crept specimens (Hv) on log [t_f.exp(-280,000/RT)] for tube and annealed/tempered plate (broken line) and for quenched/tempered plate (solid line). As with the stress rupture behaviour (Figs. 2 and 7), the hardness values for all three heat treatments are very similar in tests of long duration, even though the hardness of the quenched/tempered plate exceeds the values recorded for the other two materials in tests of short duration [12].

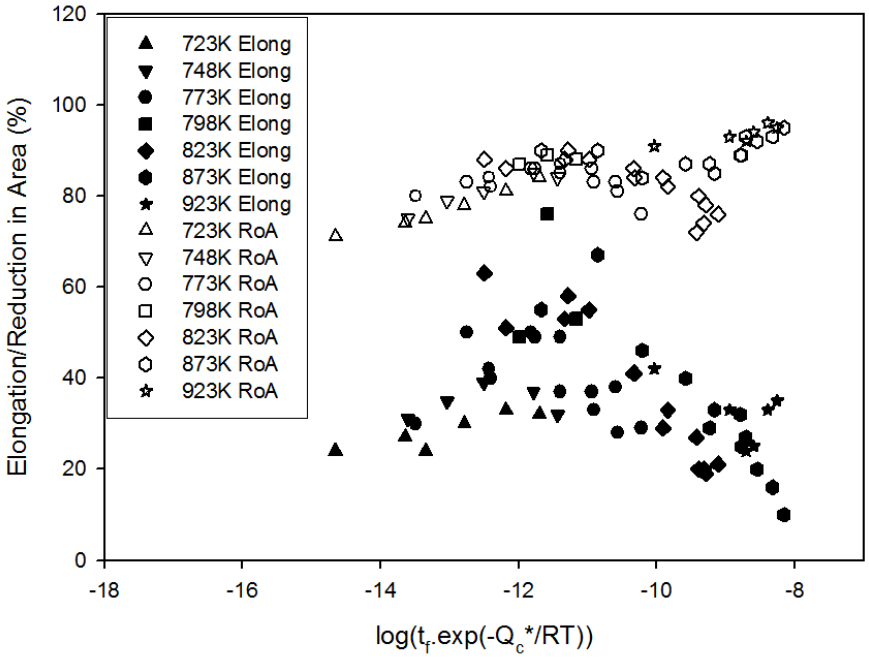

Fig.10. The dependencies of the reduction in area (RoA) and total strain to failure (ε_f) on log [$t_f.\exp(-Q_c^*/RT)$], with Q_c^*=280kJmol^{-1}, for Grade 22 steel tube.

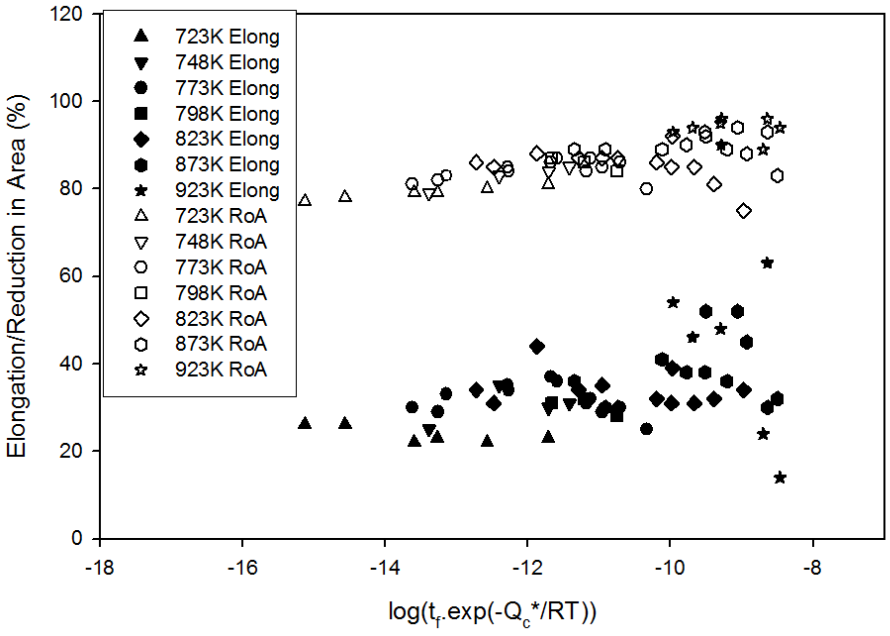

Fig.11. The dependencies of the reduction in area (RoA) and total strain to failure (ε_f) on log [$t_f.\exp(-Q_c^*/RT)$], with Q_c^*=280kJmol^{-1}, for annealed and tempered Grade 22 plate.

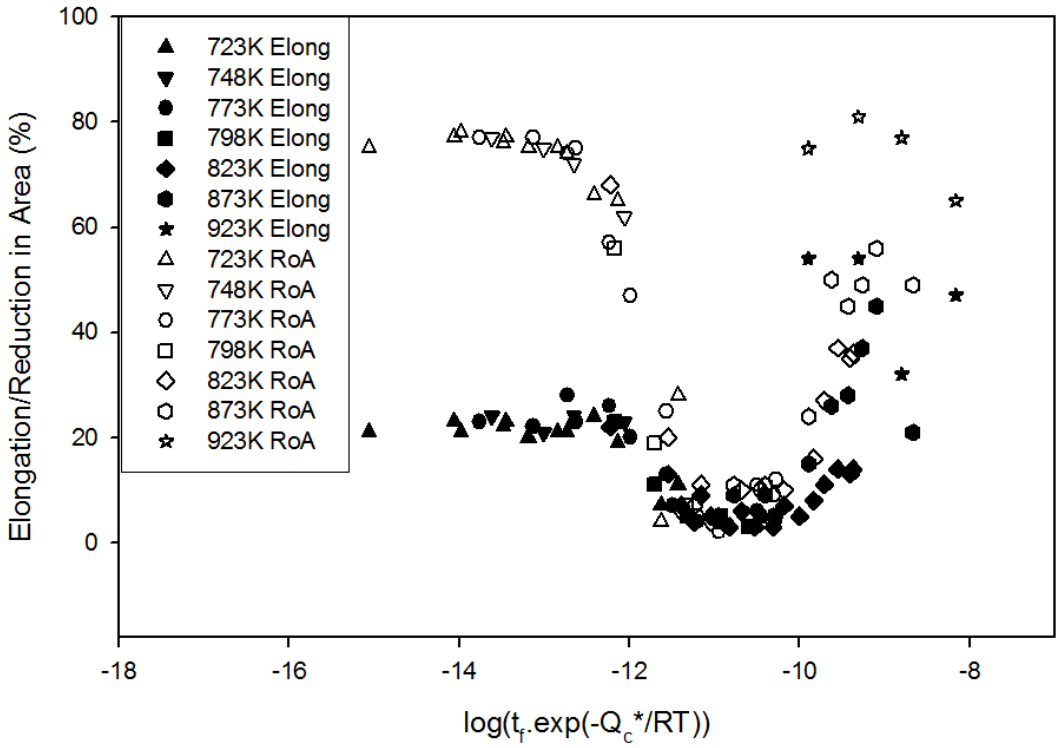

Fig.12. The dependencies of the reduction in area (RoA) and total strain to failure (ε_f) on log [t_f.exp(-Q_c^*/RT)], with Q_c^*=280kJmol^{-1}, for quenched and tempered Grade 22 plate.